General Disclaimer

One or more of the Following Statements may affect this Document

- This document has been reproduced from the best copy furnished by the organizational source. It is being released in the interest of making available as much information as possible.

- This document may contain data, which exceeds the sheet parameters. It was furnished in this condition by the organizational source and is the best copy available.

- This document may contain tone-on-tone or color graphs, charts and/or pictures, which have been reproduced in black and white.

- This document is paginated as submitted by the original source.

- Portions of this document are not fully legible due to the historical nature of some of the material. However, it is the best reproduction available from the original submission.

Produced by the NASA Center for Aerospace Information (CASI)

X-660-76-58

PREPRINT

NASA TM X- 71083

GAMMA-RAY AND MICROWAVE EVIDENCE FOR TWO PHASES OF ACCELERATION IN SOLAR FLARES

(NASA-TM-X-71083) GAMMA-RAY AND MICROWAVE EVIDENCE FOR TWO PHASES OF ACCELERATION IN SOLAR FLARES (NASA) 30 p HC $4.00 CSCL 03B

N76-20056

Unclas
G3/92 22158

T. BAI
R. RAMATY

MARCH 1976

GODDARD SPACE FLIGHT CENTER
GREENBELT, MARYLAND

GAMMA-RAY AND MICROWAVE EVIDENCE FOR TWO PHASES OF ACCELERATION IN SOLAR FLARES

T. Bai*
Department of Physics and Astronomy
University of Maryland
College Park, Maryland 20742 U.S.A.

AND

R. Ramaty
Goddard Space Flight Center
Greenbelt, Maryland 20771 U.S.A.

*Research supported by NASA Grant 21-002-316
at the University of Maryland, College Park.

ABSTRACT

Relativistic electrons in large solar flares produce gamma-ray continuum by bremsstrahlung and microwave emission by gyrosynchrotron radiation. Using observations of the 1972, August 4 flare, we evaluate in detail the electron spectrum and the physical properties (density, magnetic field, size, and temperature) of the common emitting region of these radiation. We also obtain information on energetic protons in this flare by using gamma-ray lines. From the electron spectrum, the proton-to-electron ratio, and the time dependences of the microwave emission, the 2.2 MeV line and the gamma-ray continuum, we conclude that in large solar flares relativistic electrons and energetic nuclei are accelerated by a mechanism which is different from the mechanism which accelerates $\leq$ 100 keV electrons in flares.

I. INTRODUCTION

Extensive measurements of solar radio emissions, X-rays, and interplanetary energetic particles have firmly established the fact that charged particles are copiously accelerated in solar flares. Even though the detailed flare acceleration mechanism is not known, the data tends to support the suggestion (Wild, Smerd and Weiss, 1963; deJager 1969; Frost and Dennis, 1971) that the acceleration process consists of at least two phases. The first phase, or flash phase, accelerates mainly electrons up to energies of several hundred keV. These electrons produce Type III radio bursts, impulsive 10 to 100 keV X-ray emissions, microwave bursts, and EUV bursts (e.g. Kane, 1974); streams of energetic electrons detected in interplanetary space are also believed to be due to this acceleration phase (Lin, 1974). Because the total energy in electrons accelerated in the first phase constitutes a large fraction of the energy of the flare (Lin, 1974; Hudson, Jones, and Lin, 1975), only very efficient first order acceleration mechanisms can be responsible for this phase of acceleration.

The second phase of acceleration occurs in a smaller fraction of flares than does the first phase, and it accelerates ions to tens and hundreds of MeV and electrons to relativistic energies. This acceleration phase is associated with Type II and Type IV bursts, and produces the fluxes of ions and electrons of energies greater than several MeV observed in interplanetary space. Microwave and hard X-ray bursts are also produced during second phase acceleration. But as pointed out by Frost and Dennis (1971), X-ray bursts produced

during this phase are different in character than those associated with the first phase. The acceleration of the ions and the electrons in the second phase is probably due to the passage of shock fronts in the solar atmosphere.

Gamma-ray emission in the energy interval from 0.35 to 8 MeV, containing both lines and continuum, has been observed during the 3B flare of 1972, August 4 (Chupp et al., 1973; 1975; Suri et al., 1975). The implications of the line emissions have been investigated most recently by Ramaty, Kozlovsky, and Lingenfelter (1975), and interpretations of the continuum have been given by these authors, by Suri et al. (1975), and by Bai and Ramaty (1975). The most likely mechanism for the production of continuum emission in the above energy region is bremsstrahlung of accelerated electrons. The lines are due to nuclear interactions of energetic protons and ions with ambient solar atmosphere.

In the present paper we show that unique information on the two phases of acceleration in solar flares can be obtained by treating the gamma-ray data together with the X-ray and microwave observations of the 1972, August 4 flare. The fact that the gamma-ray continuum from the 1972, August 4 flare may contain this information was first pointed out to us by A. N. Suri, E. L. Chupp, D. J. Forrest and C. Reppin (private communication, 1974). The gamma-ray continuum and the hard X-ray emission from this flare define an electron spectrum over the broad energy range from about 20 keV to several MeV which shows the effects of the two phases of acceleration. The spectral flattening above $\sim$ 0.8 MeV (Figure 1) suggests that below this energy the electrons are accelerated in the first acceleration phase, while above this energy

they come from the second phase. Furthermore, a detailed treatment of gyrosynchrotron radiation reveals that radio emission above about 25 GHz is produced by electrons in the MeV region. Therefore, the microwave emission should be more closely related to the gamma-ray continuum than to the X-ray data; this fact is borne out by the observations. Finally, the existence of spectral lines in the gamma-ray data gives information on the number, spectrum and time dependence of accelerated nuclei in the flare; we find that the data is consistent with the acceleration of nuclei in the second phase.

In section II we calculate in detail the bremsstrahlung produced by the interaction of accelerated electrons with the ambient solar atmosphere. Using these calculations, we deduce the number and spectrum of electrons in the flare region which produce the observed continuum emission in the X-ray and gamma-ray bands. In section III we calculate the gyrosynchrotron radiation of these electrons. By fitting these calculations to the microwave and millimeter emissions observed from the August 4 flare (Croom and Harris, 1973), we deduce the magnetic field, the ambient density, the size, and the temperature of the emitting region. We take into account all the known absorption mechanisms (e.g. Ramaty, 1973), and we find that the microwave emission is supressed at low frequencies mainly by selfabsorption and free-free absorption. With these absorption mechanisms taken into account, we show that the apparent discrepancy between solar microwave and hard X-ray bursts (Peterson and Winckler, 1959) is satisfactorily resolved. In section IV we investigate the time dependences of the various emissions. We

find that the time profile of the number of accelerated nuclei in the flare is more closely associated with the time profile of electrons accelerated in the second phase rather than in the first phase. We summarize our results in section V.

II. HIGH-ENERGY CONTINUUM EMISSION

The instantaneous photon production rate per unit energy at a photon energy ϵ, owing to electron-proton bremsstrahlung, is given by

$$q(\epsilon) = n \int_{\epsilon}^{\infty} dE\ N(E)\ c\beta\ \frac{d\sigma}{d\epsilon}\ (E,\epsilon), \tag{1}$$

where n is the ambient proton density, N(E) is the instantaneous number of accelerated electrons per unit kinetic energy interval around E, $c\beta$ is the electron velocity, and $\frac{d\sigma}{d\epsilon}\ (E,\epsilon)$ is the unscreened differential cross section for electron-proton bremsstrahlung (Koch and Motz, 1959, Equation 3BN),

$$\frac{d\sigma}{d\epsilon}\ (E,\epsilon) = \alpha r_o^2\ \frac{p'}{p\epsilon}$$

$$\cdot \left\{ \frac{4}{3} - 2\gamma\gamma' \left(\frac{p^2 + p'^2}{p^2 p'^2} \right) + \frac{k\gamma'}{p^3} + \frac{k'\gamma}{p'^3} - \frac{kk'}{pp'} + \right. \tag{2}$$

$$\left. + L \left[\frac{8}{3} \frac{\gamma\gamma'}{pp'} + \frac{\epsilon^2 (\gamma^2\gamma'^2 + p^2 p'^2)}{(mc^2)^2 p^3 p'^3} + \frac{\epsilon/mc^2}{2pp'} \left(k \frac{\gamma\gamma' + p^2}{p^3} - k' \frac{\gamma\gamma' + p'^2}{p'^3} + \right. \right. \right.$$

$$\left. \left. \left. \frac{2\epsilon\gamma\gamma'}{mc^2 p^2 p'^2} \right) \right] \right\}.$$

Here m is the mass of the electron, $\alpha = 1/137$, $r_o = 2.82 \times 10^{-13}$ cm, $\gamma = E/mc^2 + 1$, $\gamma' = \gamma - \epsilon/mc^2$, $p = (\gamma^2 - 1)^{\frac{1}{2}}$, $p' = (\gamma'^2 - 1)^{\frac{1}{2}}$, and

$$L = 2 \ln \frac{\gamma\gamma' + pp' - 1}{\epsilon/mc^2} \quad ; \quad k = \ln \frac{\gamma + p}{\gamma - p} \quad ; \quad k' = \ln \frac{\gamma' + p'}{\gamma' - p'} \ . \tag{3}$$

For energies below 2 MeV, Equation (2) is multiplied by the Elwert correction factor, f_E, (Koch and Motz, 1959, Equation II-6)

$$f_E = \frac{\beta \left[1 - \exp\left\{-2\pi/(137\beta)\right\}\right]}{\beta' \left[1 - \exp\left\{-2\pi/(137\beta')\right\}\right]}, \qquad (4)$$

where $\beta' = (\gamma'^2 - 1)^{\frac{1}{2}}/\gamma'$.

In addition to electron-proton interactions, bremsstrahlung is also produced in the interactions of accelerated electrons with heavier nuclei (mainly He) and with ambient electrons. For a He/H ratio of 0.07 (Cameron, 1973) the contribution of electron-helium bremsstrahlung is 28% of the electron-proton bremsstrahlung at the same electron energy. Electron-electron bremsstrahlung is negligible in the non-relativistic region, but it becomes comparable to electron-proton bremsstrahlung in the relativistic domain (Akhiezer and Berestetskii, 1965). Therefore, we neglect it below an electron energy of 0.7 MeV, and take it to be the same as electron-proton bremsstrahlung at higher energies. We have chosen the transition energy somewhat arbitrarily at 0.7 MeV, because there is no detailed theory for electron-electron bremsstrahlung in the mildly relativistic domain. A different transition energy in the range 0.5 to 1 MeV does not change our results substantially.

Using Equations (1), (2), (3), (4), and the above assumptions, we have evaluated the photon spectra produced by various electron distributions. From these results we deduce the differential electron number in the flare region which produces by bremsstrahlung a photon spectrum that fits the observations shown in Figure 1. The shaded

area in this figure shows the range of variability of the observed hard X-ray flux in the time interval from 06:23 UT to 06:30 UT (van Beek et al., 1973), and the error bars represent the average observed gamma-ray flux over the time interval from 06:24 UT to 06:33 UT (Suri et al., 1975). As can be seen, two sets of observations agree reasonably well. The solid line in Figure 2 is the differential electron number in the flare region that produces the photon flux shown by the solid line in Figure 1.

The quantity nN(E) for the deduced electron spectrum is given by

$$nN(E) = \begin{cases} 3.3 \times 10^{44}\, E^{-2.4}, & E < 0.1 \text{ MeV} \\ 2.6 \times 10^{43}\, E^{-3.5}, & 0.1 \text{ MeV} < E < 0.8 \text{ MeV} \\ 1.4 \times 10^{42}\, \exp(-E/4), & E > 0.8 \text{ MeV} \end{cases} \qquad (5)$$

where E is in MeV and nN is in electrons cm^{-3} MeV^{-1}. The most prominent features of this electron spectrum are the break at an energy of about 100 keV and the excess or bump at energies greater than about 0.8 MeV. The break at ~ 100 keV, first observed by Frost (1969), is a rather common feature in solar X-ray bursts. This break is probably due to the diminishing efficiency of the first-phase acceleration mechanism that produces electrons in the energy range up to several hundred keV. On the other hand, the bump above ~ 0.8 MeV is a novel feature, probably caused by a population of electrons accelerated by the second-phase mechanism. A similar bump can also be seen in the observations of Gruber et al. (1973) of the 1967, May 23 flare.

In order to investigate the uniqueness of the high-energy bump

in the deduced electron spectrum, we have evaluated the bremsstrahlung from an electron distribution for which the transition from the second to the third branch in Equation (5) is not so abrupt as that shown by the solid line in Figure 2. The resultant photon and electron spectra are shown by the dash-dotted lines in Figures 1 and 2, respectively. As can be seen, the solid line in Figure 1 provides a better fit to the data than the dash-dotted line. Therefore, electrons in the flare region may possess a sharp spectral change at energies from about 0.5 to 1 MeV, reflecting the transition from the first to the second acceleration phase.

The dashed line in Figure 2 is the differential proton number in the flare region deduced (Ramaty et al., 1975) from the observed gamma-ray lines at 2.2, 4.4 and 6.1 MeV (Chupp et al., 1975). Because these lines give information on the proton spectrum in the energy region between about 10 to 100 MeV, whereas the observed gamma-ray continuum is insensitive to electrons in this energy range, it is not possible to compare the proton and electron numbers at exactly the same energy. Nevertheless, with a slight extrapolation of the electron spectrum, we see that the proton-to-electron ratio at $\sim$ 10 MeV is about 100:1, a value quite similar to that found in the galactic cosmic rays. It should be pointed out that this ratio pertains to the instantaneous particle numbers, and not to the proton and electron source functions. The latter quantities, however, have direct bearing on the acceleration mechanism. They can be obtained from the instantaneous numbers by taking into account the losses suffered by the particles. These losses are given in section IV. However, the full treatment of the relationships between the instantaneous particle numbers and source functions for the 1972, August 4 flare is deferred to a subsequent paper.

In addition to the lines at 2.2, 0.5, 4.4 and 6.1 MeV, solar flares should also produce other gamma-ray lines. These lines, however, were not resolved in the 1972, August 4 spectrum because of their low relative intensities. From the results of Ramaty et al. (1975) we estimate that for this flare the combined nuclear radiation in the energy range from about 0.8 to 2.3 MeV, mainly due to lines of Ne, Mg, Si and Fe, is about 0.1 photons $cm^{-2}s^{-1}$. As can be seen from Figure 1, this radiation, if added to the calculated bremsstrahlung flux, is not inconsistent with the data.

III. MICROWAVE EMISSION

Microwave emission in solar flares is believed to be due to gyrosynchrotron emission of energetic electrons in magnetic fields of the flare (e.g. Takakura, 1967). Large flux densities of microwave emission have been observed from the 1972, August 4 flare, at 9.4, 19, 37 and 71 GHz, coincidently with the gamma-ray observations (Croom and Harris, 1973). We proceed now to evaluate the radio spectrum produced by the electron distributions deduced in section II.

For the calculation of microwave radiation from mildly relativistic electrons we use the treatments of Ramaty (1969, 1973), and Ramaty and Petrosian (1973). The following absorption and suppression effects are potentially important for solar microwave radiation: gyroresonance absorption, absorption below the plasma frequency, free-free absorption, gyrosynchrotron selfabsorption, and the Razin effect. However, as we shall show below, only gyrosynchrotron selfabsorption and free-free

absorption are important for the 1972, August 4 event.

For a radio source of volume, V, consisting of a homogeneous and isotropic population of energetic electrons, N(E), moving in a uniform magnetic field, B, the gyrosynchrotron emissivities, $j_{\pm}(\nu,\theta)$ and selfabsorption coefficients, $K_{\pm}(\nu,\theta)$, in the ordinary (+) and extraordinary (-) modes, can be written as (Ramaty, 1969, Equation 16)

$$j_{\pm}(\nu,\theta) = \frac{B}{V} \frac{e^3}{mc^2} G_{\pm}\left(\frac{\nu}{\nu_B},\theta\right) \tag{6}$$

$$K_{\pm}(\nu,\theta) = \frac{(2\pi)^2 e}{BV} H_{\pm}\left(\frac{\nu}{\nu_B},\theta\right). \tag{7}$$

Here e is the charge of the electron; ν is the frequency of the radio emission; $\nu_B = eB/(2\pi mc)$; θ is the angle between the direction of observation and the magnetic field; and

$$\left| \begin{matrix} G_{\pm} \\ H_{\pm} \end{matrix} \right| = \frac{1/4}{\cos\theta} \int_0^{\infty} dE\, N(E)/(\beta\gamma) \sum_{s=s_1}^{s_2} \frac{s}{1-\beta\cos\theta\cos\phi_s} \times$$

$$\times \left[-\beta \sin\phi_s J_s'(X_s) \pm \left(\cot\theta - \beta \frac{\cos\phi_s}{\sin\theta}\right) J_s(X_s) \right]^2 \tag{8}$$

$$\times \left| -(\nu_B/\nu)^2 \beta\gamma^2 \frac{mc^2}{N(E)} \frac{d}{dE}\left(\frac{N(E)}{\beta\gamma^2}\right) \right|^{1},$$

where $X_s = s\beta\sin\theta\sin\phi_s/(1-\beta\cos\theta\cos\phi_s)$, $s_{1,2} = (\nu/\nu_B)\gamma(1 \pm \beta\cos\theta)$, and $\cos\phi_s = [1 - s\nu_B/(\gamma\nu)]/(\beta\cos\theta)$.

The free-free absorption coefficient is given by (Ramaty and Petrosian, 1972)

$$K_{ff} = 10^{-2} n_e^2/(\nu^2 T^{3/2}) \{ 17.7 + \ln(T^{3/2}/\nu) \}, \tag{9}$$

where n_e and T are the density and temperature of the ambient free electrons. Using Equations (6) through (9), we can write the radio flux density at Earth as

$$F = \frac{A}{R^2}\left\{ \frac{j_+}{K_+} \left[1 - \exp(- \tau_+ L)\right] + \frac{j_-}{K_-} \left[1 - \exp(-\tau_- L)\right] \right\}, \quad (10)$$

where A and L are the area and depth of the radio source, respectively, and R = 1 A.U. We have evaluated Equation (10) numerically, and the results are shown in Figures 3 and 4.

In Figure 3 we show the flux density at Earth in the absence of absorption ($\tau_+ L \to 0$ and $\tau_- L \to 0$). Spectrum A is due to the electron distribution $N(E) = 2.6 \times 10^{43} E^{-3.5}$ with a high-energy cutoff at E = 0.8 MeV; spectrum B is produced by the same distribution with no high-energy cutoff and spectrum C is due to the distribution $N(E) = 1.4 \times 10^{42} \exp(-E/4\ \mathrm{MeV})$. The electrons below 0.1 MeV given by the first branch of Equation (5) produce negligible radio emission for $\nu > 5\nu_B$. Because at lower harmonics the emission is strongly absorbed, we do not have to take into account the contribution of these electrons.

The open dots in Figure 4 represent the average microwave flux density obtained by integrating the observed (Croom and Harris, 1973) flux densities over the gamma-ray measurement time (1972, August 4, 06:24 to 06:33 UT). When these data are compared with the calculated spectra of Figure 3, two results become apparent: The microwave flux density flattens at high frequencies ($\nu \geq 3 \times 10^{10}$ Hz), as expected from the presence of component C; there is evidence for strong absorption at lower frequencies ($\nu \leq 15$ GHz).

The calculated lines in Figure 4 were obtained from Equation (10) with finite absorption. Component A, due to $N(E) = 2.6 \times 10^{43} \times E^{-3.5}$ with a high energy cutoff at 0.8 MeV, is absorbed both by gyrosynchrotron selfabsorption and free-free absorption. For simplicity we have applied only free-free absorption to component C; however, the addition of selfabsorption does not change the total spectrum because selfabsorption is important only at frequencies where the contribution of component C is negligible. We used the following parameters: B = 415 gauss, $n = 7.1 \times 10^{10}$ cm^{-3}, $A = 1.6 \times 10^{19}$ cm^2(0.9 arc minutes), and $L/T^{3/2} = 0.41$. If $L \simeq A^{1/2} = 4 \times 10^9$ cm, then $T = 4.5 \times 10^6$K. These values represent reasonable estimates for the physical conditions of the acceleration region. We note that there is no inconsistency between the total number of electrons deduced from the radio emission and that obtained from the X- and gamma-ray emissions. As already pointed out by Holt and Ramaty (1969), the apparent inconsistency found by Peterson and Winckler (1959) is removed mainly by gyrosynchrotron selfabsorption.

For the above density, temperature and magnetic field, the plasma frequency, ν_p, the gyroresonance absorption frequency, $\nu_{gr} = 4\nu_B$, and the Razin cutoff frequency, $\nu_R = 20\ n_e/B$ (Ramaty, 1973), are 2.4, 4.6 and 3.4 GHz, respectively. Because these values are lower than the observed turnover frequency of $\sim$ 15 GHz, the above three mechanisms cannot contribute significantly to the suppression of microwave emission for the 1972, August 4 flare.

Castelli et al. (1974) have recently analyzed the microwave emission from the 1972, July 31 flare. Contrary to our conclusions for

the 1972, August 4 flare, these authors find that the dominant low-frequency suppression mechanism for the July 31 event is gyroresonance absorption. Since the August 4 burst at ~ 15 GHz was larger by a factor of ~ 100 than the July 31 burst, it is possible that these two conclusions are not mutually inconsistent. We point out, however, that Castelli et al. (1974) use an incorrect formula for ν_{sa}, the turnover frequency for gyrosynchrotron selfabsorption. According to Ramaty (1973), the formula $\nu_{sa} \simeq 5.3 \times 10^7 \, B^{1/2} (F_m/\Omega)^{2/5}$, where ν_{sa} is in Hz, B is in gauss, F_m is in solar flux units and Ω is in (arc minutes)^2, gives a good fit to the detailed numerical calculations; the formula used by Castelli et al. (1974) has a smaller numerical coefficient by about a factor of 2. Using the above formula for ν_{sa}, we find for B = 415 gauss, $F_m = 2 \times 10^4$ flux units, and $\Omega = 0.8$ (arc minutes)^2 that $\nu_{sa} \simeq 10^{10}$ Hz, in reasonable agreement with the numerical calculations presented in Figure 3.

IV. TIME DEPENDENCES

The observed time dependences of the X-ray emission in the energy range 29 to 41 keV (van Beek et al., 1973), of the gamma-ray flux in the range 0.35 to 8 MeV (Suri et al., 1975), and of the microwave emission at 37 GHz (Croom and Harris, 1973) are shown in Figure 5. The variation in time of the X-rays depends on the time profile of electrons of several tens of keV in the flare region. On the other hand, the time dependence of the gamma rays is determined by the variation in time of electrons of energies greater than hundreds of keV; as can be seen in Figure 4, radio emission at 37 GHz is also due to

electrons in this energy range. Indeed, as seen in Figure 5, the general rise time of both the continuum gamma rays and 37 GHz radio emission (~ 4 minutes) is longer than that of the X-rays (~ 2 minutes). This result provides support to the suggestion made on the basis of spectral information in section II, that electrons above several hundreds of keV are accelerated by a different mechanism than the mechanism which accelerates lower energy electrons. We should point out, however, that there is good observational correlation between the individual peaks of the X-ray, gamma-ray, and microwave time profiles, as can be seen in Figure 5. Therefore, the first-phase and second-phase acceleration mechanisms should be closely related. For example, the first-phase mechanism could serve as an injection source for the second mechanism. This possibility is supported by the total number of electrons in the two components: from Figure 2 we calculate that the number of electrons in the high-energy component is only 0.1% of the number of electrons in the lower energy component above 20 keV.

If different acceleration mechanisms are responsible for the acceleration of low- and high-energy electrons, it is of considerable interest to determine which of the two mechanisms accelerates protons and nuclei. The time profile of the nucleonic component in the flare region can be deduced directly from the observed time profile of the 2.2 MeV line. This line is due to the reaction $n + p \rightarrow d + \gamma$, where the neutrons are the products of nuclear reactions of energetic protons and nuclei in the flare region (Ramaty et al., 1975).

The error bars on the 2.2 MeV gamma-ray time profile shown in Figure 5 are the measured intensities of this line (Chupp et al., 1975). The solid, dashed, and dotted lines are calculated time profiles of the 2.2 MeV line obtained by using the results of Wang and Ramaty (1974). The solid line is obtained by assuming that the instantaneous number of nuclei in the flare region has the same time dependence as that of the observed 0.35 to 8 MeV gamma rays. The dashed and dotted lines are obtained by assuming that the time dependence of the nuclei is the same as that of the 29 to 41 keV X-rays. For the solid and dotted lines we used a photospheric ^{3}He abundance, $^3\mathrm{He/H} = 5 \times 10^{-5}$; for the dashed line, $^3\mathrm{He/H} = 0$.

As can be seen, the measured time profile of the 2.2 line is in good agreement with the calculated result shown by the solid line. The dashed and dotted lines, however, give poorer fits to the data, independent of the amount of ^{3}He in the photosphere. (A smaller amount of ^{3}He in the photosphere results in a slower loss of neutrons and hence a longer delay of the 2.2 MeV line). This result implies that the nuclei are probably accelerated by the second-phase mechanism.

The individual peaks in the time profiles of the X-rays, continuum gamma rays and microwaves shown in Figure 5 have decay times of about 30 seconds. These decay times can be due to energy losses of electrons in the flare region if the energy loss time of the relevant electrons are shorter than the observed decay times, or due to the escape of electrons from the emitting region.

In Figure 6 we show the energy loss times, $E/(dE/dt)$, for protons

and electrons in a fully ionized plasma of density, temperature, and magnetic field as deduced in section III: $n = 7.1 \times 10^{10}$ cm^{-3}, $T = 4.5 \times 10^{6}$K, and B = 415 gauss. The energy loss rate, dE/dt, is due to Coulomb collisions for protons, and due to both Coulomb collisions and synchrotron losses for electrons. We have used the results of Trubnikov (1965) for electron Coulomb collisions, and those of Ginzburg and Syrovatskii (1964) for proton Coulomb collisions. The transition at $\sim$ 1 MeV in energy loss time for protons is due to the fact that the proton velocity at this energy is comparable to the electron thermal speed for $T = 4.5 \times 10^{6}$ K. For electron synchrotron losses we have used the results of Ginzburg and Syrovatskii (1964). The maximum, at $\sim$ 10 MeV, in the energy loss time for electrons is due to these losses.

As can be seen from Figure 6, the energy loss time of $\leq$ 50 keV electrons which produce the 29 to 41 keV X-rays is less than about 1 second. Therefore, the observed decay times of $\sim$ 30 seconds of the individual peaks of these X-rays could be due to collisional losses. This conclusion is different from that of Brown and Hoyng (1975), who have suggested that the observed time variations could be due to betatron acceleration and deceleration in a medium of density 4×10^{7} cm^{-3} and magnetic field 12 gauss. These low values, however, are inconsistent with the density and field deduced in section III from the microwave and X- and gamma-ray data. The energy-loss time of $\sim$ 2 MeV electrons which produce 37 GHz microwaves and continuum gamma rays is $\sim$ 70 seconds. For these electrons, escape from the emitting region may play an important role in determining the observed time profile.

V. SUMMARY

We have calculated the X-ray, gamma-ray continuum and microwave emissions from the 1972, August 4 flare. By comparing these calculations with the data, we can deduce the number and spectrum of the energetic electrons, the ambient density, n, the magnetic field, B, the area of the radio source, A, and the temperature of the emitting region, T. The energy spectrum and absolute value of the product nN(E) are given in Equation (5) and Figure 2. For the rest of the parameters we find that $n = 7.1 \times 10^{10}$ cm^{-3}, B = 415 gauss, $A = 1.6 \times 10^{19}$ cm^2 ($\Omega = 0.8$ (arc minutes)^2), and $T = 4.5 \times 10^6$K.

The deduced energy spectrum of the electrons supports the suggestion (Wild et al., 1963; deJager, 1969; Frost and Dennis, 1971) of two acceleration phases. For the 1972, August 4 flare, the first phase accelerates electrons up to several hundred keV; the second phase accelerates electrons to at least several MeV and protons to energies greater than several tens of MeV. From observations of gamma-ray lines (Chupp et al., 1973; 1975) and the theory of line production in solar flares (Ramaty et al., 1975), we obtain a proton-to-electron ratio at about 10 MeV of $\sim$ 100:1. This result is consistent with the fact that the second phase acceleration produces a larger flux of protons than electrons (Sturrock, 1974).

Microwave emission at frequencies greater than 25 GHz in the 1972, August 4 flare is produced by electrons in the MeV region which also produce the gamma-ray continuum. The spectral flattening, caused

by the transition from the first-phase to the second-phase acceleration, produces observable flattenings in both the gamma-ray continuum and microwave spectra. Below about 20 GHz the microwave emission is strongly absorbed by selfabsorption and free-free absorption.

The observed time profile of the 2.2 MeV gamma-ray line is consistent with the assumption that the number of accelerated nuclei has the same time dependence as the electron number at energies greater than several hundred keV. On the other hand, the 2.2 MeV time profile, calculated by assuming that the nuclei have a similar time dependence as the X-rays below $\sim$ 100 keV, precedes the data by about 100 seconds. This result lends further support to the two phase acceleration hypothesis and gives information on the time lag between the two phases.

REFERENCES

Akhiezer, A. I. and Berestetskii, V. B.: 1965, Quantum Electrodynamics, Interscience Publisher, New York.

Bai, T. and Ramaty, R.: 1975, Conference Papers, 14th International Cosmic Ray Conference, Munich, W. Germany, p. 1662.

Brown, J. C. and Hoyng, P.: 1975, Astrophys. J. 200, 734.

Cameron, A. G. W.: 1973, Space Sci. Rev. 15, 121.

Castelli, J. P., Guidice, D. A., Forrest, D. J., and Babcock, R. R.: 1974, J. Geophys. Res. 79, 889.

Chupp, E. L., Forrest, D. J., Higbie, P. R., Suri, A. N., Tsai, C., and Dunphy, P. P.: 1973, Nature 241, 333.

Chupp, E. L., Forrest, D. J., and Suri, A. N.: 1975, Proc. of IAU/ COSPAR Symposium No. 68, Solar Gamma-, X- and EUV Radiations, edited by S. Kane, p. 341.

Croom, D. L. and Harris, L. D. J.: 1973, World Data Center Report UAG-28, Pt. I., p. 210.

deJager, C.: 1969, Cospar Symposium on Solar Flares and Space Research, ed. C. deJager and Z. Svestka (Amsterdam: North-Holland Publishing), p. 1.

Frost, K. J.: 1969, Astrophys. J. Letters 158, L159.

Frost, K. J. and Dennis, B. R.: 1971, Astrophys. J. 165, 655.

Ginzburg, V. L. and Syrovatskii, S. I.: 1964, The Origin of Cosmic Rays, Macmillan and Co., New York.

Gruber, D. E., Peterson, L. E., and Vette, J. I.: 1973, High Energy Phenomena on the Sun, edited by R. Ramaty and R. G. Stone, NASA SP-342 (National Aeronautics and Space Administration, Washington, D. C.), p. 147.

Holt, S. S. and Ramaty, R.: 1969, Solar Phys. 8, 119.

Hudson, H. S., Jones, T. W., and Lin, R. P.: 1975, Proc. of IAU/COSPAR Symposium No. 68, Solar Gamma-, X-, and EUV Radiations, edited by S. Kane, p. 425.

Kane, S. R.: 1974, Coronal Disturbances, IAU Symposium No. 57 (D. Reidel, Dordrecht--Holland), p. 105.

Koch, H. W. and Motz, J. W.: 1959, Rev. Mod Phys. 31, 920.

Lin, R. P.: 1974, Space Sci. Rev. 16, 189.

Peterson, L. E. and Winckler, J. R.: 1959, J. Geophys. Res. 64, 697.

Ramaty, R.: 1969, Astrophys. J. 158, 753.

Ramaty, R.: 1973, High Energy Phenomena on the Sun, edited by R. Ramaty and R. G. Stone, NASA Sp-342 (National Aeronautics and Space Administration, Washington, D. C.), p. 188.

Ramaty, R., Kozlovsky, B., and Lingenfelter, R. E.: 1975, Space Sci. Rev. 18, 341.

Ramaty, R. and Petrosian, V.: 1972, Astrophys. J. 178, 241.

Sturrock, P. A.: 1974, Coronal Disturbances, IAU Symposium No. 57 (D. Reidel, Dordrecht--Holland), p. 437.

Suri, A. N., Chupp, E. L., Forrest, D. J., and Reppin, C.: 1975, Solar Phys. 43, 415.

Takakura, T.: 1967, Solar Phys. 1, 304.

Trubnikov, B. A.: 1965, Rev. Plasma Phys. 1, 105.

van Beek, H. F., Hoyng, P., and Stevens, G. A.: 1973, World Data Center Report UAG-28, Pt. II, p. 319

Wang, H. T. and Ramaty, R.: 1974, Solar Phys. 36, 129.

Wild, J. P., Smerd, S. F., and Weiss, A. A.: 1963, Ann. Rev. Astron. Astrophys. 1, 291.

FIGURE CAPTIONS

Figure 1. The observed hard X-ray and gamma-ray continuum from the 1972, August 4 flare. The shaded area is based on the data of van Beek et al. (1973) and includes all their spectra between 0623 and 0630 UT. The data points are from Suri et al. (1975). The solid line represents the bremsstrahlung spectrum calculated from the electron spectrum shown by the solid line in Figure 2. The dash-dotted line is the additional photon spectrum obtained from the additional electron spectrum given by the dash-dotted line in Figure 2.

Figure 2. Electron and proton differential numbers for the 1972, August 4 flare. The electrons produce by bremsstrahlung the photon spectra shown in Figure 1. For the power law spectrum (including the dash-dotted part) we ignore electron-electron interactions, while for the exponential spectrum we take into account these interactions as described in the text. The proton spectrum is obtained from gamma-ray line observations.

Figure 3. Radio flux densities from the electron spectra shown in Figure 2. The spectrum A is from $N(E) = 2.6 \times 10^{43} E^{-3.5}/n$, $0.1 < E < 0.8$ MeV; B is from the same N(E) as A except that there is no high-energy cutoff on E; C is from $N(E) = 1.4 \times 10^{42} \exp(-E/4)/n$ with no low or high-energy cutoffs.

Figure 4. Radio flux densities from the components A and B defined in Figure 3, with the effects of selfabsorption and free-free absorption. The circles are based on the data of Croom and Harris (1973). The fit to the data implies that the angular size and temperature of the radio source are 0.9 arc minutes and 4.5×10^6 K.

Figure 5. Time dependences of radiations of the 1972 August 4, flare. The three upper lines are the measured time profiles of X-rays (29 ~ 41 keV), gamma rays (0.35 ~ 8 MeV), and microwaves (37 GHz). The error bars in the lower part of the figure represent the measured intensities of the 2.2 MeV line. The solid, dashed, and dotted lines are calculated time profiles of the 2.2 MeV line. The solid line is obtained by assuming that the instantaneous number of nuclei in the flare region has the same time dependence as that of the observed 0.35 to 8 MeV gamma rays. The dashed and dotted lines are obtained by assuming that the time dependence of the nuclei is the same as that of the 29 to 41 keV X-rays. For the solid and dotted lines we used a photospheric ^{3}He abundance $^3He/H = 5 \times 10^{-5}$; for the dashed line, $^3He/H = 0$.

Figure 6. Energy loss times, $E/(dE/dt)$, of electrons and protons in the medium with $n = 7.1 \times 10^{10}$ cm^{-3}, B = 415 gauss, and $T = 4.5 \times 10^6$K.

PRECEDING PAGE BLANK NOT FILMED

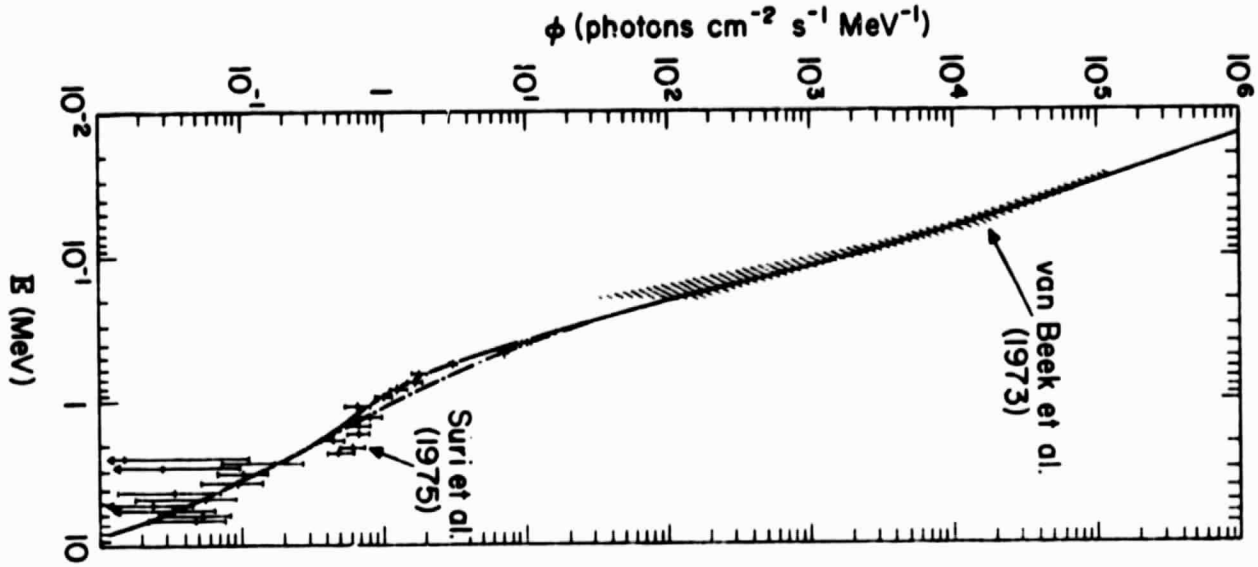

Figure 1

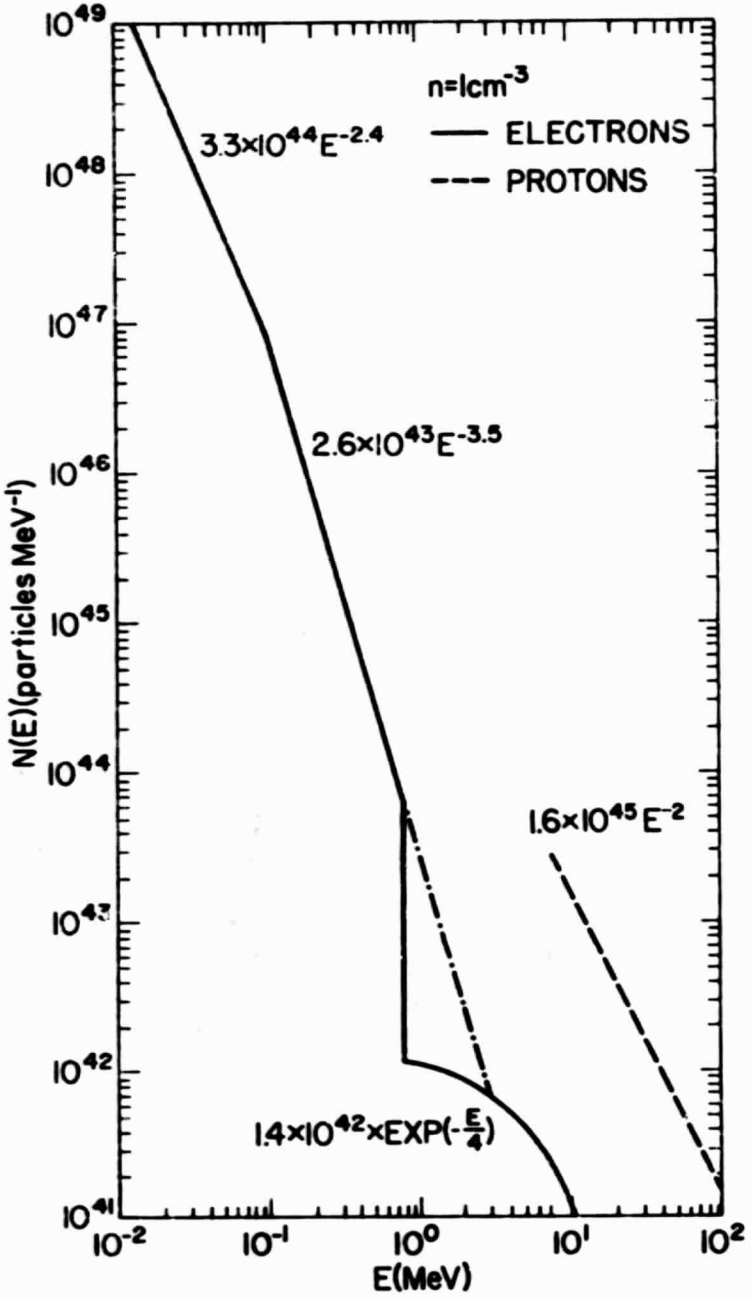
n=1cm⁻³
ELECTRONS
PROTONS
3.3×10⁴⁴E⁻²·⁴
2.6×10⁴³E⁻³·⁵
1.6×10⁴⁵E⁻²
1.4×10⁴²×EXP(-E/4)
N(E)(particles MeV⁻¹)
E(MeV)
10⁴⁹
10⁴⁸
10⁴⁷
10⁴⁶
10⁴⁵
10⁴⁴
10⁴³
10⁴²
10⁴¹
10⁻²
10⁻¹
10⁰
10¹
10²

Figure 2

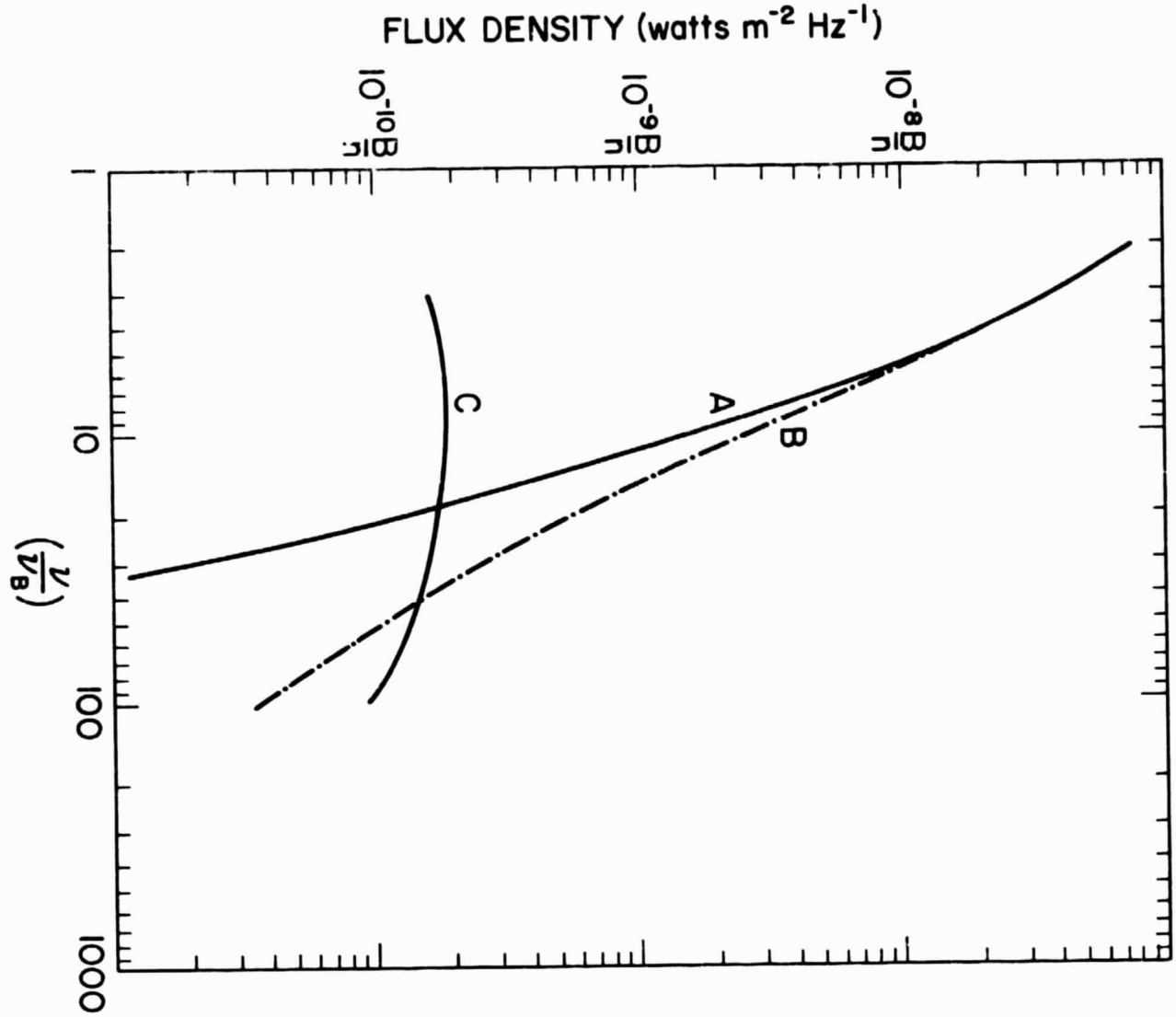
FLUX DENSITY (watts m^{-2} Hz^{-1})
10^{-10}
10^{-9}
10^{-8}
1
10
100
1000
$(\frac{\nu}{\nu_8})$
A
B
C

Figure 3

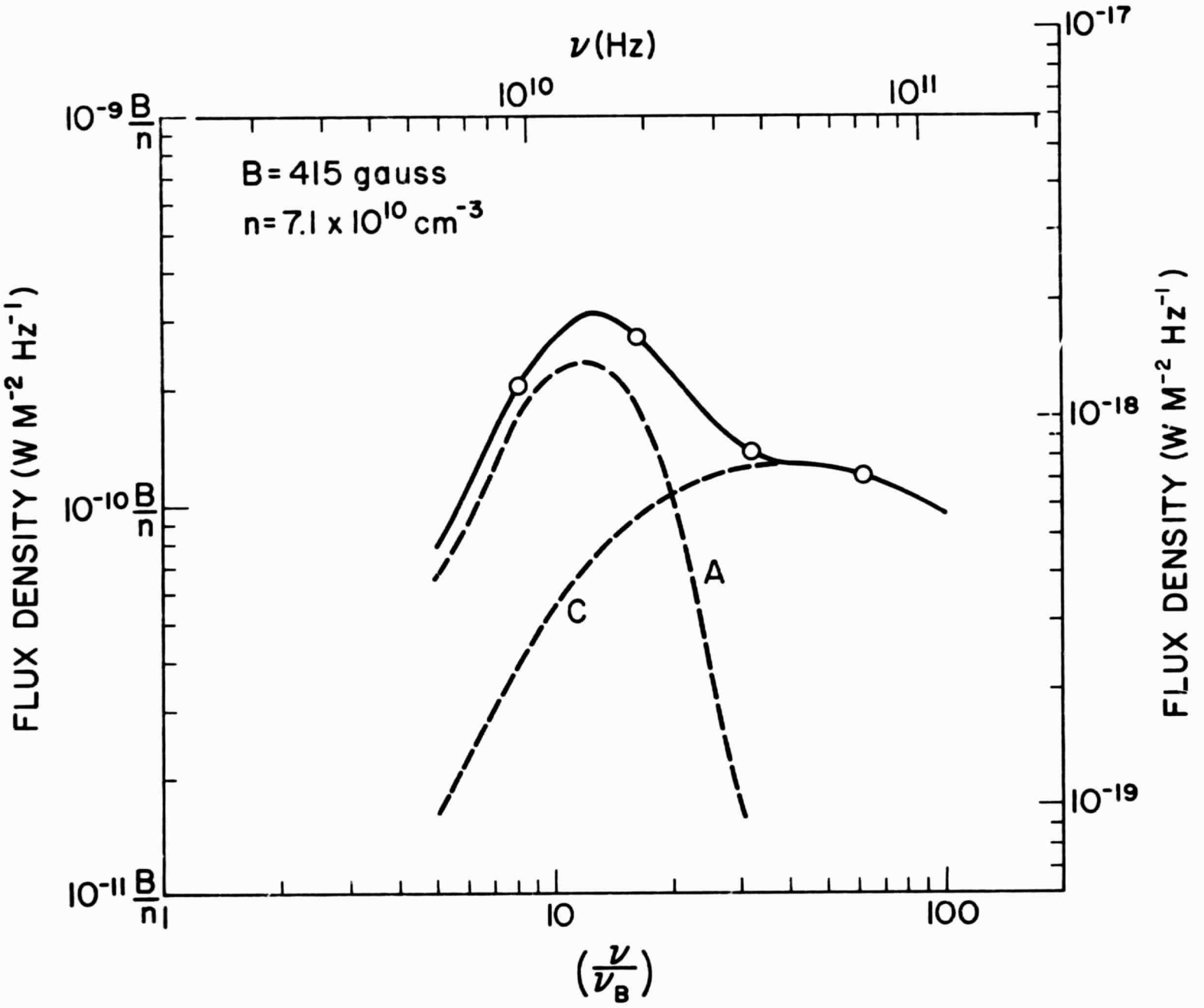
ν(Hz)
10^10
10^11
B = 415 gauss
n = 7.1 x 10^10 cm^-3
10^-9 B/n
10^-10 B/n
10^-11 B/n
FLUX DENSITY (W M^-2 Hz^-1)
10^-17
10^-18
10^-19
FLUX DENSITY (W M^-2 Hz^-1)
A
C
10
100
(ν/ν_B)

Figure 4

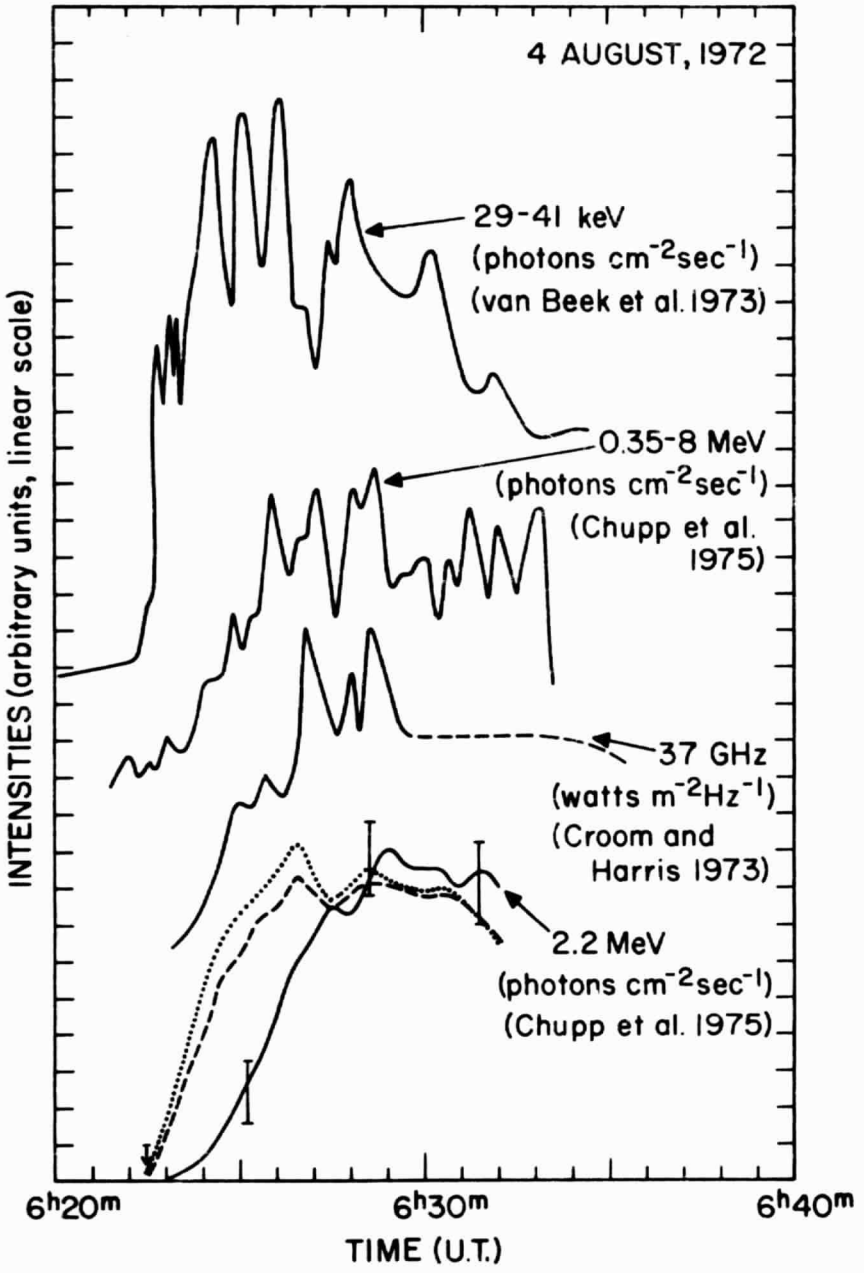
4 AUGUST, 1972
29-41 keV
(photons cm^{-2}sec^{-1})
(van Beek et al. 1973)
0.35-8 MeV
(photons cm^{-2}sec^{-1})
(Chupp et al. 1975)
37 GHz
(watts m^{-2}Hz^{-1})
(Croom and Harris 1973)
2.2 MeV
(photons cm^{-2}sec^{-1})
(Chupp et al. 1975)
INTENSITIES (arbitrary units, linear scale)
6h20m
6h30m
6h40m
TIME (U.T.)

Figure 5

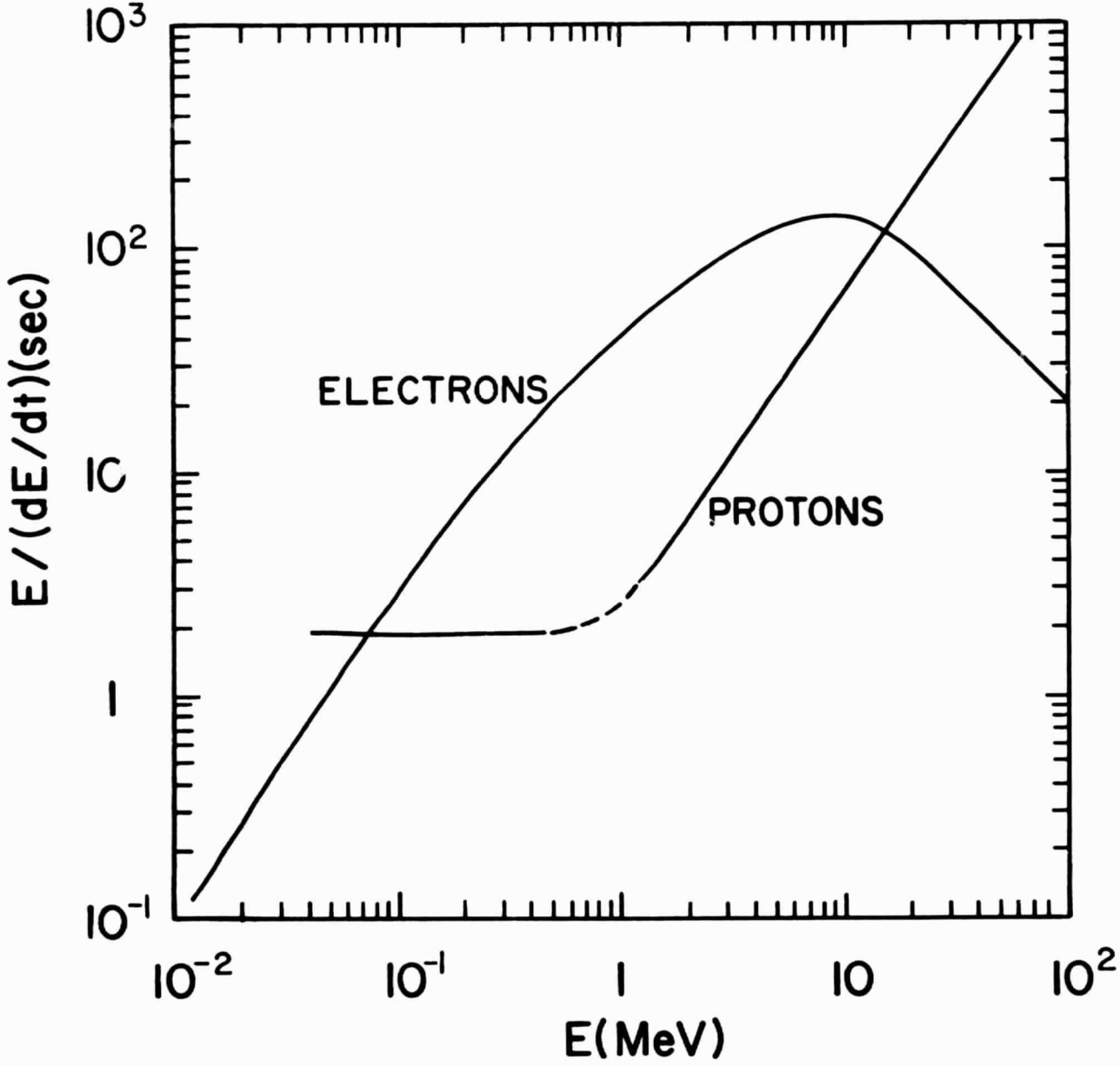
10^3
10^2
10
1
10^{-1}
E/(dE/dt)(sec)
ELECTRONS
PROTONS
10^{-2}
10^{-1}
1
10
10^2
E(MeV)

Figure 6